Noninvasive Optical Imaging of *Staphylococcus aureus* Bacterial Infection in Living Mice Using a Bis-Dipicolylamine-Zinc(II) Affinity Group Conjugated to a Near-Infrared Fluorophore

W. Matthew Leevy,[†] Seth T. Gammon,[‡] James R. Johnson,[†] Andrew J. Lampkins,[†] Hua Jiang,[†,§] Manuel Marquez,[△,⊥] David Piwnica-Worms,[‡] Mark A. Suckow,[#] and Bradley D. Smith*[,†]

Department of Chemistry and Biochemistry and Walther Cancer Research Center, 251 Nieuwland Science Hall, University of Notre Dame, Notre Dame, Indiana 46556, The Molecular Imaging Center, Mallinckrodt Institute of Radiology, Washington University School of Medicine, 510 South Kingshighway Boulevard, Campus Box 8225, St. Louis, Missouri 63110, Key Laboratory of Photochemistry, Institute of Chemistry, Chinese Academy of Sciences, Beijing 100080, China, NIST Center for Theoretical and Computational Nanosciences, Gaithersburg, Maryland 20899, Harrington Department of Bioengineering, Arizona State University, Tempe, Arizona 85287, and Freimann Life Sciences Center, University of Notre Dame, Notre Dame, Indiana 4655. Received October 8, 2007; Revised Manuscript Received December 12, 2007

Optical imaging of bacterial infection in living animals is usually conducted with genetic reporters such as light-emitting enzymes or fluorescent proteins. However, there are many circumstances where genetic reporters are not applicable, and there is a need for exogenous synthetic probes that can selectively target bacteria. The focus of this study is a fluorescent imaging probe that is composed of a bacterial affinity group conjugated to a near-infrared dye. The affinity group is a synthetic zinc (II) coordination complex that targets the anionic surfaces of bacterial cells. The probe allows detection of *Staphylococcus aureus* infection (5×10^7 cells) in a mouse leg infection model using whole animal near-infrared fluorescence imaging. Region of interest analysis showed that the signal ratio for infected leg to uninfected leg reaches 3.9 ± 0.5 at 21 h postinjection of the probe. Ex vivo imaging of the organs produced a signal ratio of 8 for infected to uninfected leg. Immunohistochemical analysis confirmed that the probe targeted the bacterial cells in the infected tissue. Optimization of the imaging filter set lowered the background signal due to autofluorescence and substantially improved imaging contrast. The study shows that near-infrared molecular probes are amenable to noninvasive optical imaging of localized *S. aureus* infection.

INTRODUCTION

Optical imaging of bacterial infection in living animals is emerging as a powerful method to study preclinical models of infectious disease. In most cases, genetic reporter systems such as light-emitting luciferase enzymes, or fluorescent proteins like GFP, have been employed with some notable success (*1*). However, pathogenic bacteria in their native environments do not express endogenous optical reporters. Furthermore, numerous microbes are not amenable to genetic manipulation or DNA transfection. In these cases, alternative optical imaging strategies must be developed such as the use of exogenous synthetic probes that selectively target the bacteria. While the most immediate application of these synthetic probes is the study of preclinical infection models in mice, they also have long-term clinical potential for imaging bacteria in shallow tissue. For example, prosthetic materials like mesh grafts or catheters are common sites of colonization by invasive bacteria such as MRSA (methicillin-resistant *Staphyloccus aureus*) (*2*), but they are difficult systems to image.

To date, only a small number of bacterial targeting probes have been reported for any imaging modality, and very few have been studied in vivo. A key design component is the bacteria targeting group, and previous studies have employed antibodies (*3*), lectins (*4*), sugars (*5*), antibiotic drugs (*6–8*), and peptides (*9*). Antibodies are popular, since they can bind tightly to specific molecular targets on the surfaces of both Gram-positive and Gram-negative bacterial cells (*10*). While antibodies have the potential advantage of high specificity, their large molecular size (~150 kD) is a limitation for in vivo imaging because of slow tissue diffusion and blood clearance rates.

A more general way to target bacteria is to employ cationic molecules that are electrostatically attracted to the negatively charged cells (*11, 12*). The negative surface charge is a characteristic feature of nearly all bacterial membranes, and results from the high fraction of anionic phospholipids and related amphiphiles (*13*). For example, the plasma membrane which surrounds the Gram-positive bacterium *Staphylococcus aureus* is composed of approximately 75% anionic phosphatidylglycerol. Extending from this membrane are anionic glycerophosphate polymers called lipoteichoic acids that weave through and anchor the surrounding peptidoglycan cell wall (*14*). Gram-negative bacteria such as *Escherichia coli* are differentiated by the presence of a second outer bilayer membrane. The external leaflet of this outer membrane is composed of lipopolysaccharide whose core structure, known as lipid A, contains two anionic phosphates (*15*). The anionic surfaces of bacteria are in contrast to the exterior membrane surfaces of most healthy mammalian cells, which contain primarily zwit-

* smith.115@nd.edu, ph: +1 (574) 631 8632, fax: +1 (574) 631 6652.
[†] Department of Chemistry and Biochemistry and Walther Cancer Research Center, University of Notre Dame.
[‡] Washington University School of Medicine.
[§] Chinese Academy of Sciences.
[△] NIST Center for Theoretical and Computational Nanosciences.
[⊥] Arizona State University.
[#] Freimann Life Sciences Center, University of Notre Dame.

10.1021/bc700376v CCC: $40.75
Published on Web 02/09/2008

terionic phospholipids and thus have a near-neutral charge (*16*). For imaging purposes, a drawback with cationic peptides is their propensity to penetrate (and be retained by) mammalian cells (*17, 18*), while a limitation with antimicrobial peptides is poor signal-to-noise since they actively degrade the bacterial cell membrane target (*19*).

We have discovered that zinc (II) coordination complexes with dipicolylamine (DPA) ligands exhibit remarkably selective affinities for anionic cell membranes (*20*). For example, DPA-Zn(II) based probes allow fluorescent visualization of apoptotic mammalian cells, as they expose anionic phosphatidylserine during the programmed cell death process (*21*). In addition, these DPA-Zn(II) probes are highly selective stains for bacteria even in the presence of human epithelial cells (*22*). The specific focus of this study is fluorescent probe **1** which contains a DPA-Zn(II) affinity group conjugated to a near-infrared (NIR) carbocyanine fluorophore (ex. 794 nm, em. 810 nm). NIR fluorophores are optimal for in vivo imaging purposes given the favorable tissue penetration properties of photons at these wavelengths (*23*). In a preliminary report, we showed that **1** can identify infection sites in living mice, the first demonstration of in vivo bacterial detection using a fluorescent probe (*24*). We now describe a detailed optical imaging investigation of *S. aureus* infection using region of interest analysis to characterize the pharmacokinetics of probe uptake and clearance from the whole animal. We also provide biodistribution and histology data that measures organ and cell selectivity. Overall, we find that **1** is an effective *in vivo* optical imaging probe for localized infection of *S. aureus* in living mice.

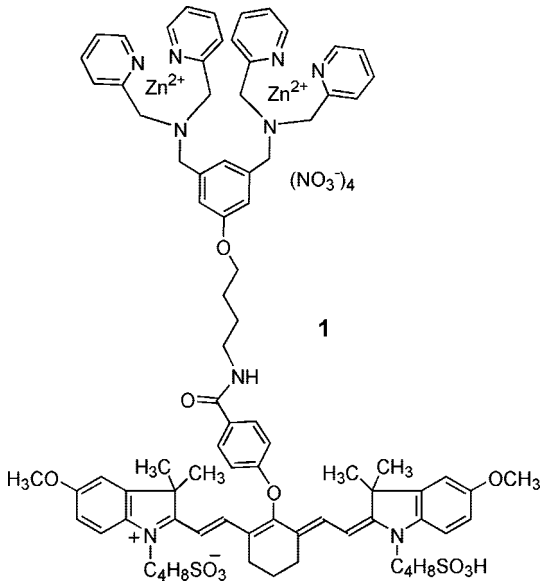

EXPERIMENTAL PROCEDURES

Synthesis. Compound **1** was prepared as previously reported (*24*).

In Vivo Leg Infection Model. An aliquot of *Staphylococcus aureus* NRS11 (5×10^7 colony forming units (CFUs) in 50 μL of Luria–Bertani growth media) was injected intramuscularly into the muscles that overlay the tibia bone in a posterior leg of an athymic nude mouse (strain nu/nu, Taconic, New York). It is worth noting that this anatomical location is not the thigh, which is closer to the body of the mouse. The same location on the contralateral leg was injected with 50 μL of LB media as a vehicle control. The infection was allowed to incubate for 6 h before intravenous injection with probe **1** via the tail vein. After imaging experiments, the mice were anesthetized and euthanized by cervical dislocation.

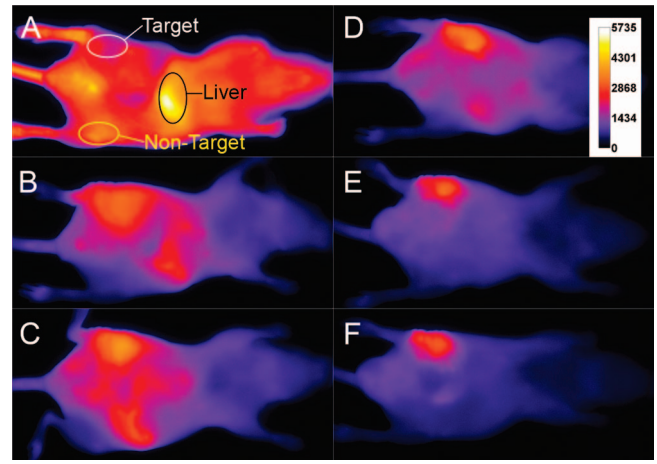

Figure 1. Optical images of a mouse with a *S. aureus* infection in the left posterior leg. Images were acquired following intravenous injection of probe **1** (75 μL of a 1 mM stock) at 0 h (A), 3 h (B), 6 h (C), 12 h (D), 18 h (E), and 21 h (F). Calibration bar (a.u.) applies to all images in the montage. Frame A shows labels for each region of interest (ROI): target (T), non-target (NT), and liver (L).

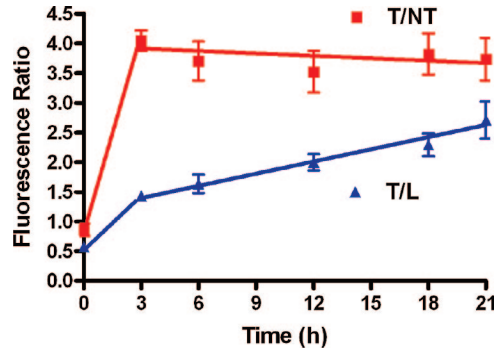

Figure 2. Target to nontarget (T/NT) and target to liver (T/L) fluorescence ratios at each imaging time point ($n = 4$; error bars are standard error of the mean). The lines are provided to guide the eye.

In Vivo Fluorescence Imaging. Imaging was achieved by placing an anesthetized mouse (1.5% isofluorane inhalation) inside a Kodak 4000MM imaging station configured for epi-illumination. The entire animal was irradiated with filtered light of wavelength 755 ± 20 nm, and a 16-bit image of emission intensity at 830 ± 10 nm was collected by a CCD camera during a 60 s acquisition period (F-stop = 2.4, focal plane 2.5 mm, FOV 200 mm no binning). In some cases, the mouse was also imaged using a filter set with excitation at 720 ± 10 nm and emission at 790 ± 35 nm. Mice were imaged before and immediately after injection of **1**, and at subsequent time points as detailed in the text.

Image Preparation and Quantitative Analysis. Images were processed using the *ImageJ 1.37v* program available for free download at http://rsb.info.nih.gov/ij/. Figures 1, 4, 6, and 7 were prepared as follows. First, the original 16-bit images (presented as panels in each figure) were sequentially opened and then converted to an image stack using the "convert images to stack" software command. Next, the stack of images was background-subtracted using the rolling ball algorithm (radius = 500 pixels) that is a feature of the software. This tool calculates the average pixel intensity of any signal emanating from a "non-mouse" region of the image, and then subtracts this calculated value from every pixel in the image. The radius was selected to exceed the maximum width of the mouse; otherwise, the mouse itself will be included in the background calculation. Next, the image stack was set to the "Fire"

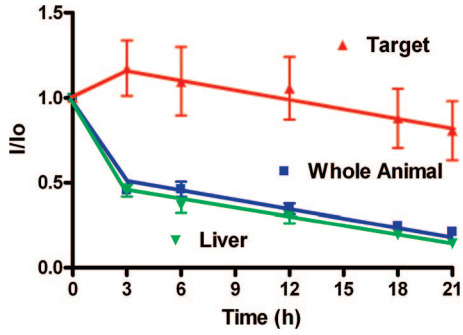

Figure 3. Fluorescence emission time course for the infection target, whole animal, and liver ROIs ($n = 4$; error bars are standard error of the mean). The lines are provided to guide the eye.

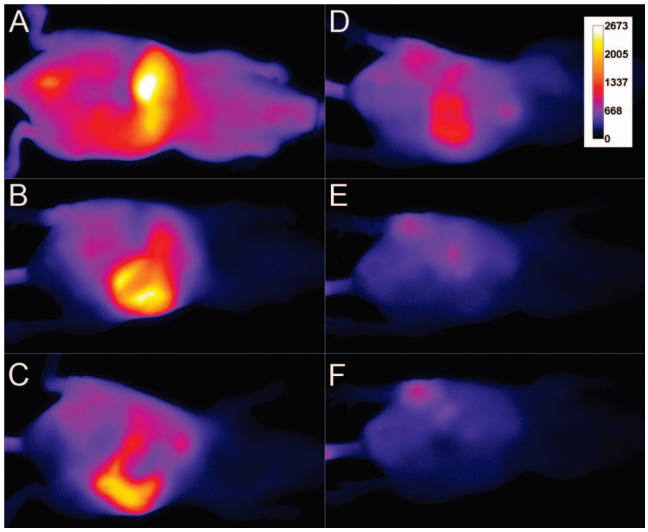

Figure 4. Optical images of a mouse with a *S. aureus* infection in the left posterior leg. Images were acquired following intravenous injection of a low dose of probe **1** (75 μL of a 0.2 mM stock) at 0 h (A), 3 h (B), 6 h (C), 12 h (D), 18 h (E), and 21 h (F). Calibration bar (a.u.) applies to all images in the montage.

fluorescence intensity scale (under "Lookup Tables" menu), which color-codes the fluorescence counts contained in each pixel. After that, the stack of images was converted to a montage using the "convert stack to montage" command. At this point, region of interest (ROI) analysis was performed by selecting a circle ROI from the *ImageJ* tool bar, and drawing it to circumscribe the appropriate anatomical location of each mouse, as shown in Figure 1. The average pixel intensities of the target (T), nontarget (NT), and liver (L) were measured by *ImageJ* (CTRL-M) and recorded for each mouse in *Excel 2003*. In addition, an ROI was drawn around the whole mouse (excluding the target site) and the integrated density recorded. Statistical analysis was performed to acquire the average of each ROI ($n = 4$) with the standard error of the mean (SEM), and the resulting values plotted in *Graphpad Prizm 4*. Two-way ANOVA analysis was also performed in *GraphPad* version 4 to calculate the *p*-values reported in the text. After ROI analysis, a calibration bar was added to the montage using the "calibration bar" command in the *ImageJ* program.

Biodistribution. After imaging studies, the mice were anesthetized by isofluorane inhalation (1.5%) and euthanized by cervical dislocation. The major organs were dissected, placed on a glass plate, and imaged as described above. The biodistribution image was analyzed in *ImageJ* by first subtracting the background (rolling ball method, 100 pixel width). Manual regions of interest (ROIs) were drawn around each organ, and

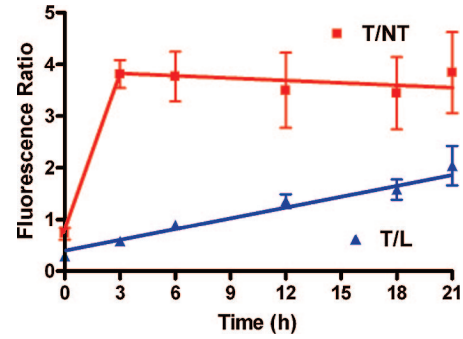

Figure 5. Target to nontarget (T/NT) and target to liver (T/L) fluorescence ratios at each imaging time point after injection with a 0.2 mM stock of **1** ($n = 4$, error bars are standard error of the mean).

the mean pixel intensity calculated for each. ROIs were drawn around the discrete site of infection. The averages for each organ ($n = 3$) and each infected site ($n = 4$) were calculated and plotted as detailed above.

Histology. The first analysis used mice with a 9 h infection in one of the posterior legs, but no treatment with probe **1**. Tissue was sampled, including the skin, subcutis, and muscle from the leg which had been administered bacteria; a similar sample was also obtained from the contralateral uninfected leg. The tissue was fixed in 10% neutral buffered formalin for 24 h and then transferred to 70% ethanol. Following embedding in paraffin, tissue was sectioned at 4–5 μm and stained with hematoxylin and eosin. The second analysis used mice that had been infected with bacteria and also injected with probe **1**. Sections at 10 μm from the infected leg and the uninfected contralateral leg were stained with a Texas Red-labeled antibody to *Staphyloccus aureus* protein A (250 μL of a 100 μg/mL solution in buffer: 5 mM TES (*N*-tris(hydroxymethyl)methyl-2-aminoethanesulfonic acid), 145 mM NaCl, pH = 7.4), (Abcam Inc., Goa pAb to protein A (TR) ab7247–1). Microscopy was performed at 600× magnification on a Nikon Eclipse 2000TE microscope with a Photometrics Cascade 512B camera to aquire 16 bit images. Each image was processed using the *ImageJ* software suite. A control in vitro microscopy study confirmed that the Texas-red labeled antibody targets the surface of the *S. aureus*, as expected, with no emission in the Cy7 filter set.

RESULTS AND DISCUSSION

In Vivo Imaging. The bacteria were injected into the muscles that overlay the tibia bone in a posterior leg of athymic nude mice. This infection model was chosen for the following reasons (*1*): (a) The posterior leg is well-separated from all major organs, and bacterial migration from the site is slow, thus reducing any confusion as to the origin of the fluorescent signal. (b) The lack of hair produces less scattering of the light. (c) The inhibited immune system simplifies interpretation of the imaging and histology data.

A cohort of four mice was each infected with a bolus of 5×10^7 colony forming units (CFUs) of *S. aureus* NRS11 in a 50 μL aliquot of Luria–Bertani (LB) growth media. The contralateral leg was injected with LB alone to serve as the vehicle control. After a 6 h incubation, each mouse was injected intravenously, via the tail vein, with probe **1** (75 μL of an aqueous 1 mM stock solution). Assuming a blood volume of 1 mL, the final concentration of **1** in the blood was approximately 75 μM or about 4 mg/kg. Each animal was subsequently imaged on its ventral side at 0, 3, 6, 12, 18, and 21 h using a Kodak 4000MM Imaging Station designed to acquire 16 bit planar fluorescence images. The images were subsequently processed using the *ImageJ* V1.37 software suite (see methods). It is important to note that colors in these images do not represent

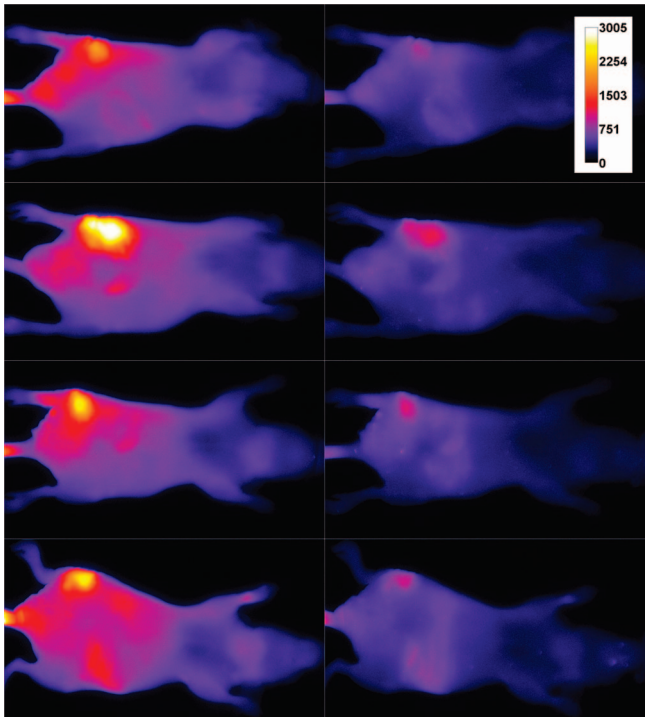

Figure 6. Optical images of four mice each with a *S. aureus* infection in the left posterior leg and acquired 21 h postinjection of probe **1** (75 μL of a 1 mM stock). Left column: animals were imaged using an excitation of 755 nm and emission of 830 nm. Right column: the same animals were imaged using an excitation of 720 nm and emission of 790 nm. Calibration bar (a.u.) applies to all images in the montage.

wavelengths of light, but rather the fluorescence intensity of each pixel in the image.

In Figure 1 are typical fluorescence images (ex: 755, em: 830 nm) obtained for one mouse during the time course of one experiment. Immediately after injection with **1**, there is a bright, confluent fluorescence emanating from most parts of the animal. A region of interest (ROI) analysis was derived from the average pixel intensities at the three anatomical locations shown in frame A: the target leg infection site (T), the contralateral leg as a nontarget site (NT), and the liver (L). At time zero, the target to nontarget (T/NT) fluorescence ratio was 0.85 ± 0.1 ($n = 4$, standard error of the mean), indicating that less probe diffuses through the infected leg relative to the control leg immediately following injection. The cause of this small decrease is unknown, but it may be the result of *S. aureus* induced ischemic damage to the local vasculature, as observed for other Gram-positive microbes (*25*). Localization of **1** can be observed at the target site within 3 h postinjection, and the image continues to sharpen as the probe clears from the mouse body over the subsequent 18 h. Figure 2 shows the average target to nontarget (T/NT) and target to liver (T/L) fluorescence ratios for the cohort of four mice at each imaging time point during the study. The lines that connect the points are to guide the eye and do not represent a mathematical fit. A salient point is that the T/NT ratio reaches a value close to 4 after just 3 h and is sustained for the remainder of the experiment (at 21 h, T/NT $= 3.9 \pm 0.5$, $n = 4$). The T/L ratio also rises quickly during the first 3 h, and then continues to increase slowly with time such that T/L $= 2.7 \pm 0.4$ ($n = 4$) at 21 h.[1] It is important to appreciate the difference between

[1]The values of T/NT and T/L reported here compare favorably with an imaging study that utilized radiolabeled antimicrobial peptides and reported T/NT ratios as high as 4.1 ± 0.7 (*30*). A value for T/L could not be determined, since most of the signal originated from the body of the mouse and not the target site.

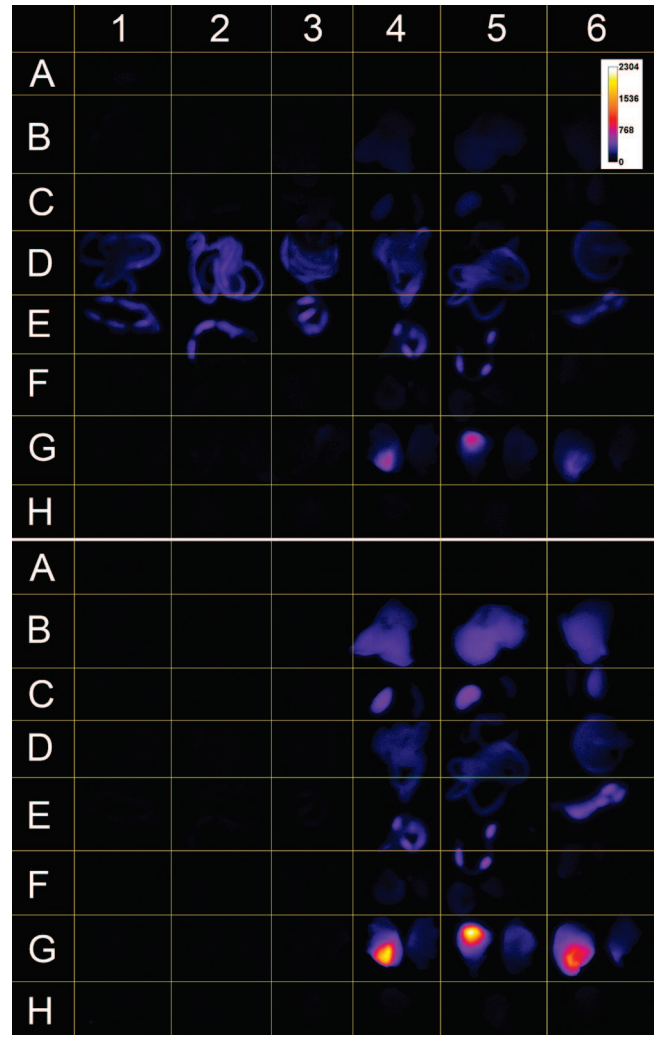

Figure 7. Ex vivo image of mouse tissues from three uninfected mice (columns 1–3) and three infected mice that were injected with **1** (colums 4–6). The organs and blood are given in the following rows of Figure 5: (A) blood, (B) liver, (C) kidney (left) and spleen (right), (D) small intestine, (E) large intestine, (F) lungs (left) and heart (right), (G) left and right posterior leg tissue, and (H) brain. Images were acquired with the 720/790 nm (top frame) and 755/830 nm (bottom) filter sets. Calibration bar (a.u.) set for both frames.

T/NT and T/L. The T/NT ratio is a measure of targeting at the infection site relative to the contralateral control site, whereas the T/L ratio is a measure of the imaging contrast observed between the infection site and the whole mouse. Thus, while the T/NT ratio reaches a maximum in the first 3 h of imaging, the continued linear increase in T/L up to 21 h time reflects the improving contrast that helps identify the infection site relative to the mouse body.

Plotted in Figure 3 are the average changes in total fluorescence emission (I/I_o) from the target site and also the whole animal over the course of the imaging experiment ($n = 4$). These data show that the fluorescence emission from the infection site increased by approximately 20% over the first three hours of the experiment, whereas, the total animal fluorescence decreased by 50% over the same period. This indicates that most of probe **1** binds to the target within the first 3 h, and that after this initial phase, the infection site, liver, and whole animal lose fluorescence at the same apparent linear rate.

In Vivo Imaging with Lower Probe Concentration. Additional in vivo imaging studies were performed to assess the sensitivity of probe **1**. The main goal was to determine whether

useful imaging results could be obtained with a lower dose.[2] Thus, a cohort of four mice were each given a leg infection of *S. aureus* as described above, but this time they received a 5-fold lower intravenous concentration of **1** (15 μM estimated final blood concentration). As shown in Figure 4, the overall signal from the infected leg was less intense. The T/L ratio in Figure 5 increased linearly with time to reach a value of 1.9 $\pm$ 0.4 after 21 h, which is 70% of the value obtained using the higher dose of **1**. Although the signal contrast is lower, the T/NT ratio (Figure 5) mirrors the higher probe dose profile and reaches a value close to 4 after 3 h. These data indicate that the lower probe dose can be used to effectively image a leg infection because this anatomical location has an inherently low background signal that is primarily due to tissue autofluorescence. However, other infection sites, like the kidney and liver which avenues for probe clearance, would be more difficult to image at this lower probe concentration since there is a higher background signal due to some nonselective accumulation of probe.

Optimizing the Imaging Filter Set. A drawback with the popular 2D planar imaging technique used in this study is the attenuation of fluorescence signal with tissue depth. Furthermore, the photophysical properties of carbocyanine fluorophores vary with both solvent polarity and the presence of serum components of blood (*26*). Therefore, it was important to gauge image variability between separate animals and also to check how much the image quality changed with different instrument filter sets. Our previous preliminary study of probe **1** (λ_{max} abs: 794 nm, em: 810 nm) employed a 720/790 nm filter set (excitation at 720 $\pm$ 10 nm, emission at 790 $\pm$ 35 nm) (*24*); however, the imaging data reported above used a more optimal 755 $\pm$ 20/830 $\pm$ 35 nm filter set. The benefit gained by using this longer-wavelength filter set is illustrated in Figure 6, which compares images of four mice at the 21 h time point. With each animal, the *S. aureus* infection site in the left posterior leg is readily discerned, demonstrating the excellent reproducibility of probe **1**. Comparatively, the contrast using the 755/830 nm filter set (Figure 6, left column) is clearly greater for each mouse than that observed with its corresponding image in the 720/790 nm filter set (Figure 6, right column). ROI analysis confirmed that the T/NT ratio for these mice is 3.8 $\pm$ 0.4 with the 755/830 nm set, which is 36% better than the T/NT ratio of 2.8 $\pm$ 0.2 obtained with the 720/790 set ($p = 0.014$). In addition, the T/L ratio values improved from 2.3 $\pm$ 0.2 (720/790 nm set) to 2.8 $\pm$ 0.5 (755/830 nm set) for a 22% average gain ($p = 0.021$). The longer-wavelength filter set enhances contrast for two reasons. First, the deeper red 755/830 nm filter set produces increased probe excitation in deeper tissues, with a corresponding enhancement of fluorescence emission. Second, there is a lower background signal from nonprobe autofluorescence.

Ex Vivo Imaging. Ex vivo fluorescence analysis of the mouse organs was performed to assess the biodistribution of probe **1**. Three mice from the cohort in Figure 3 (i.e., treated with the higher probe concentration) were euthanized by cervical dislocation at the 21 h time point and their organs gathered to determine the distribution of probe **1** (Figure 7, columns 4–6). Three additional mice, that were neither infected nor injected, were used as controls (columns 1–3). The organs and blood were placed on a glass plate and imaged using the Kodak Imaging Station with the 720/790 nm (top frame) and 755/830 nm (bottom frame) filter sets. The fluorescent images are given in the following rows of Figure 5: (A) blood, (B) liver, (C) kidney (left) and spleen (right), (D) small intestine, (E) large intestine, (F) lungs (left) and heart (right), (G) left and right posterior leg muscle, and (H) brain. The infected tissue is immediately obvious upon inspection of row G which shows the left (infected) and right (uninfected) posterior leg muscles. The fluorescence emission emanates from one area of the leg tissue, indicating that probe **1** is localized to the initial site of bacterial injection. Moderate fluorescence intensity also emanated from the liver and small and large intestine, indicating that this is a major excretion pathway for **1**.

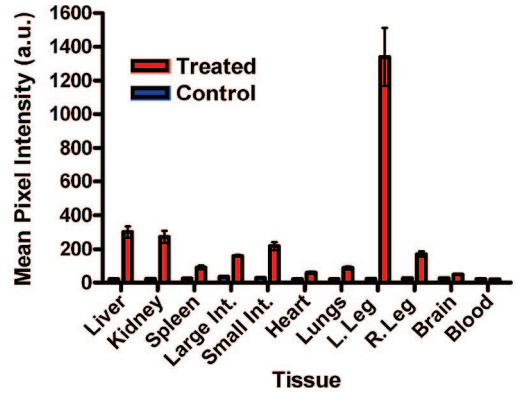

Figure 8. Ex vivo organ quantification of Figure 7 imaged with the 755/830 nm filter set ($n = 3$, error bars are the standard error of the mean).

Inspection of the images in Figure 7 shows that image contrast due to staining by probe **1** is enhanced significantly by changing the 720/790 nm filter set to the longer-wavelength 755/830 nm filter set. In particular, the strong gut autofluorescence (due to food (*27*)) for control mice 1–3 in rows D and E is almost completely eliminated, whereas the fluorescence intensity of every organ containing probe **1** is greater. In other words, the fluorescence ratio of the infected to uninfected leg (T/NT) was increased from 4.5 to 7.8 by changing to the longer-wavelength filter set. Figure 8 shows the average fluorescence intensity of the pixels in each organ as determined by ROI analysis ($n = 3$) from image taken using the optimized 755/830 nm filter set. The left leg gave about 8-fold more signal than the contralateral uninfected leg tissue. Furthermore, the infected leg had a minimum 4-fold greater intensity when compared to other organs like the liver and kidneys. Taken together, the data show that compound **1** selectively targets the leg of each animal that has a localized infection of *S. aureus*.

Histology. Two types of analyses were performed. The first was a general histological comparison of tissue sections from mice with a 9 h infection in one of the posterior legs. After fixation and embedding in paraffin, the tissue samples were sectioned at 4–5 μm and stained with hematoxylin and eosin. As expected, tissue sections from the contralateral uninfected legs were normal and showed no signs of necrosis or inflammation. Tissue sections from infected legs showed evidence of mild to moderate inflammation and some hyaline degeneration; however, there were no pyknotic nuclei or other cellular debris associated with cell death and necrosis.

The second analysis was an immunohistochemical assessment of the selectivity of probe **1** for bacterial cells. Thus, 10 μm sections were processed from the infected and uninfected leg tissue of mice that were injected with **1** (see Experimental Procedures). The sections were counter-stained with a Texas Red labeled antibody with selectivity for protein A (Abcam), an antigen present the surface of *S. aureus*. Microscopy data from one infected tissue section are shown in Figure 9. In the left panel is a phase contrast image. The region containing small dark spots (highlighted in the red box) indicates the presence

[2] A lower probe dose would, of course, lower the chance of chemical toxicity. While a complete toxicity study has not yet been conducted, it is worth noting that the nude mice easily tolerate the presence of probe **1** (4 mg/kg) for at least 24 h, as judged by their continued grooming and nesting activities.

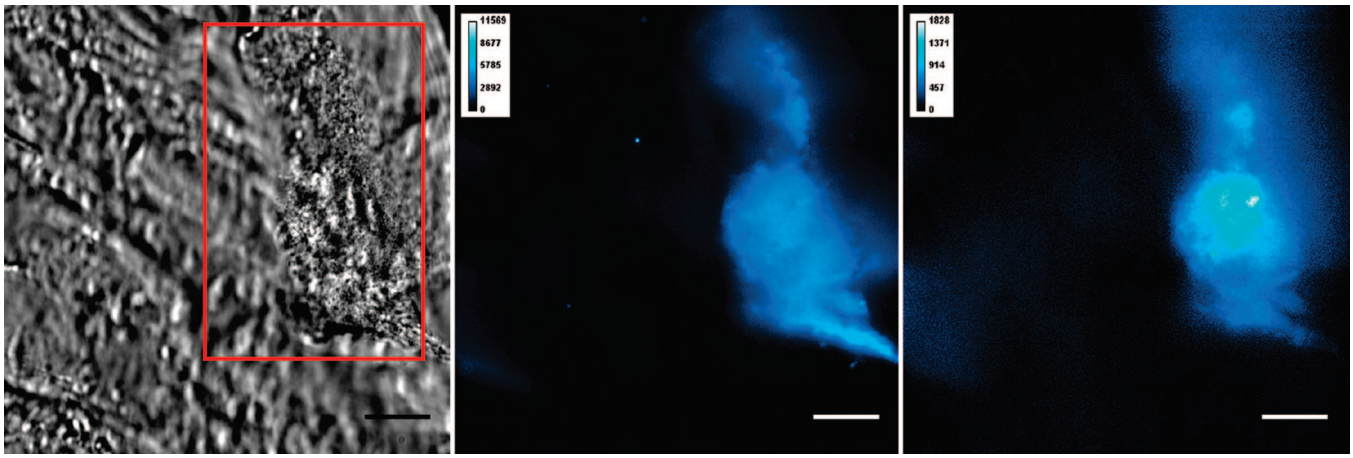

Figure 9. Histological section of infected leg muscle as viewed at 600× in the phase contrast (left), red (center), and NIR Cy7 (right) filter sets. The red box at left designates a patch of spots that mark the presence of bacteria. Infected tissue was sectioned 21 h postinjection of **1**. Scale bar equals 20 μM for each frame. Calibration bar is in arbitrary units.

of bacterial cells. The center picture shows the same section in the red filter set (ex. HQ535/50X, em. HQ610/75m). The colocalized emission from the Texas Red antibody conjugate establishes the presence of *S. aureus*. The right panel shows the section viewed with a NIR Cy7 filter set (ex. 710/75X, em. 810/90m) that selectively detects emission from **1**. The NIR fluorescence intensity in the bacterial cluster was approximately 3-fold higher than in the surrounding tissue. Images of tissue sections from the uninfected contralateral leg of the same mouse were treated with the same antibody stain, but there was no fluorescent signal in the red (antibody) or NIR (probe) channels (data not shown).

The histology data indicate that the DPA-Zn(II) affinity group in compound **1** targets the anionic membrane surfaces of the bacteria cells and not the relatively small number of dead and dying mammalian cells in the leg tissue that surrounds the infection site. Even though the amount of muscle cell death increases as the infection progresses, we expect that probe **1** continues to act as a bacterial imaging agent for two reasons. The first pertains to the increased surface to volume ratio of bacteria compared to mammalian cells. *S. aureus* cells have a diameter of approximately 750 nm, while tubular muscle cells are considerably larger with an effective diameter of over 50 μm and a length of at least 1 mm. Thus, millions of bacteria can occupy the space of one small muscle cell, with over 2 orders of magnitude more cell surface area. Second, bacterial cell surfaces typically have a higher fraction of negatively charged lipids than do mammalian cell surfaces. In the present case, *S. aureus* membranes are about 75% phophatidylglycerol, while the typical mammalian cell has about 15% phophatidylserine (*21*).

CONCLUSIONS

Fluorescent conjugate **1** is a robust imaging probe for the detection of localized *S. aureus* infection. The probe is easily visualized at a leg infection site within 3 h of administration. The probe selectively targets the bacterial cells in the infected tissue, as judged by immunohistochemical analysis. The image contrast was lower with decreased probe dosage; however, this technical limitation can be addressed with new and brighter NIR fluorophores (*28*). The focus of this study was on the Gram-positive *S. aureus*, a common source of secondary infection in healthcare facilities (*29*); however, probe **1** can likely be used to image almost all strains of bacteria because the DPA-Zn(II) affinity group targets the anionic surfaces that are a characteristic feature of nearly all bacterial membranes. One of the future goals of this research is to noninvasively detect and monitor bacterial pathogensis in various infection models, such as the urinary tract, lungs, or brain and spine. Eventually, probe **1**, or the next-generation versions, may have clinical applications. For example, optical imaging would be a useful tool for the clinician seeking information on low-grade infections that occur in mesh grafts or catheter sites, where it is often very difficult to distinguish infection from sterile inflammation.

ACKNOWLEDGMENT

This work was supported by the NIH (GM059078 for B.D.S.) and (P50 CA94056 for D.P-W) and the Walther Cancer Research Center at Notre Dame.

LITERATURE CITED

(1) Leevy, W. M., Serazin, N., and Smith, B. D. (2007) Optical imaging of bacterial infection models. *Drug Discovery Today: Disease Models*, doi: 10.1016/j.ddmod.2007.07.001.

(2) Hirose, K., Marui, A., Nomura, T., Kaneda, K., Kimura, Y., Ikeda, T., Fujita, M., Mitsuyama, M., Tabata, Y., and Komeda, M. (2007) A novel approach to reduce catheter-related infection using sustained-release basic fibroblast growth factor for tissue regeneration in mice. *Heart Vessels 22*, 261–267.

(3) Embleton, M. L., Nair, S. P., Cookson, B. D., and Wilson, M. (2002) Selective lethal photosensitization of methicillin-resistand *Staphylococcus aureus* using a tin(IV) chlorin e6 conjugate. *J. Antimicrob. Chemother. 50*, 857–864.

(4) Holm, C., and Jespersen, L. (2003) A flow-cytometric gram-staining technique for milk-associated bacteria. *Appl. Environ. Microbiol. 69*, 2857–2863.

(5) Qu, L. W., Luo, P. G., Taylor, S., Lin, Y., Huang, W. J., Anyadike, N., Tzeng, T. R. J., Stutzenberger, F., Latour, R. A., and Sun, Y. P. J. (2005) Visualizing adhesion-induced agglutination of *Escherichia coli* with mannosylated nanoparticles. *Nanosci. Nanotechnol. 5*, 319–322.

(6) Metallo, S. J., Kane, R. S., Holmlin, R. E., and Whitesides, G. M. (2003) Using bifunctional polymers presenting vancomycin and fluorescein groups to direct anti-fluorescein antibodies to self-assembled monolayers presenting D-alanine-D-alanine groups. *J. Am. Chem. Soc. 125*, 4534–4540.

(7) Gu, H., Xu, K., Xu, C., and Xu, B. (2006) Biofunctional magnetic nanoparticles for protein separation and pathogen detection. *Chem. Commun.* 941–949.

(8) Gu, H., Ho, P.-L., Tsang, K. W. T., Wang, L., and Xu, B. (2003) Using biofunctional magnetic nanoparticles to capture vancomycin-resistant Enterococci and other gram-positive bacteria at ultralow concentration. *J. Am. Chem. Soc. 125*, 15702–15703.

(9) Lupetti, A., Nibbering, P. H., Welling, M. M., and Pauwels, E. K. J. (2003) Radiopharmaceuticals: new antimicrobial agents. *Trends Biotechnol. 21*, 70–73.
(10) Wing, L., Zhao, W., O'Donoghue, M. B., and Tan, W. (2007) Fluorescent nanoparticles for multiplexed bacteria monitoring. *Bioconjugate Chem. 18*, 297–301.
(11) Hamblin, M. R., O'Donnell, D. A., Murthy, N., Rajagopalan, K., Michaud, N., Sherwood, M. E., and Hasan, T. (2002) Polycationic photosensitizer conjugates: effects of chain length and gram classification on the photodynamice inactivation of bacteria. *J. Antimicrob. Chemother. 49*, 941–951.
(12) Berry, V., Gole, A., Kundu, S., Murphy, C. J., and Saraf, R. F. (2005) Deposition of ctab-terminated nanorods on bacteria to form highly conducting hybrid systems. *J. Am. Chem. Soc. 127*, 17600–17601.
(13) *Microbial Lipids Vol. 1.* Ratledge, C., and Wilkinson, S. G. (Eds.) Academic Press, London, 1988.
(14) Fournier, B., and Philpott, D. J. (2005) Recognition of *Staphylococcus aureus* by the innate immune system. *Clin. Microbiol. Rev. 18*, 521–540.
(15) Meredith, T. C., Aggarwal, P., Mamat, W., Linder, B., and Woodard, R. W. (2006) Redefining the requisite lipopolysaccharide structure in *Escherichia coli*. *ACS Chem. Biol. 1*, 33–42.
(16) Boon, M. J., and Smith, B. D. (2002) Chemical control of phospholipid distribution across bilayer membranes. *Med. Res. Rev. 22*, 251–281.
(17) Nekhotiaeva, N., Elmquist, A., Rajarao, G. K., Hällbrink, M., Langel, Ü., and Good, L. (2004) Cell entry and antimicrobial properties of eukaryotic cell-penetrating peptides. *FASEB J. 18*, 394–396.
(18) Bullok, K., Gammon, S. T., Violini, S., Prantner, A. M., Villalobos, V. M., Sharma, V., and Piwnica-Worms, D. (2006) Permeation peptide conjugates for in vivo molecular imaging applications. *Mol. Imaging 5*, 1–18.
(19) Lupetti, A., Welling, M. M., Mazzi, U., Nibbering, P. H., and Pauwels, E. K. J. (2002) Technetium-99m labelled fluconazole and antimicrobial peptides for imaging of *Candida albicans* and *Aspergillus fumigatus* infections. *Eur. J. Nucl. Med. 29*, 674–679.
(20) Koulov, A. V., Hanshaw, R. G., Stucker, K. A., Lakshmi, C., and Smith, B. D. (2005) Biophysical studies of a synthetic mimic of the apoptosis-detecting protein annexin V. *Isr. J. Chem. 45*, 373–379.
(21) Hanshaw, R. G., and Smith, B. D. (2005) New reagents for phosphatidylserine recognition and detection of apoptosis. *Bioorg. Med. Chem.* 5035–5042.
(22) Leevy, W. M., Johnson, J. R., Lakshmi, C., Morris, J., Marquez, M., and Smith, B. D. (2006) Selective recognition of bacterial membranes by zinc(II)-coordination complexes. *Chem. Commun.* 1595–1597.
(23) Bashkatov, A. N., Genina, E. A., Kochubey, V. I., and Tuchin, V. V. (2005) Optical properties of human skin, subcutaneous and mucous tissues in the wavelength range from 400 to 2000 nm. *J. Phys. D: Appl. Phys. 38*, 2543–2555.
(24) Leevy, W. M., Gammon, S. T., Jiang, H., Johnson, J. R., Maxwell, D. J., Jackson, E. N., Marquez, M., Piwnica-Worms, D., and Smith, B. D. (2006) Optical imaging of a bacterial infection in living mice using a fluorescent near-infrared molecular probe. *J. Am. Chem. Soc. 128*, 16476–16477.
(25) Bryant, A. E., Bayer, C. R., Chen, R. Y. Z., Guth, P. H., Wallace, R. J., and Stevens, D. L. (2005) Vascular dysfunction and ischemic desctruction: the role of streptolysin o-induced platelet/neutrophil complexes. *J. Infect. Dis. 192*, 1014–1022.
(26) Yuan, B., NanGuang, C., and Zhu, Q. (2004) Emission and absorption properties of indocyanine green in intralipid solution. *J. Biomed. Opt. 9*, 497–503.
(27) Mansfield, J. R., Gossage, K. W., Hoyt, C. C., and Levenson, R. M. (2005) Autofluorescence removal, multiplexing, and automated analysis methods for in-vivo fluorescence imaging. *J. Biomed. Opt. 10*, 41207–41215.
(28) Johnson, J. R., Fu, N., Arunkumar, E., Leevy, W. M., Gammon, S. T., Piwnica-Worms, D., and Smith, B. D. (2007) Squaraine Rotaxanes: superior substitutes for Cy-5 molecular probes for near-infrared fluorescence cell imaging. *Angew. Chem., Int. Ed. 119*, 5624–5627.
(29) Dziekan, G., Hahn, A., Thune, K., Schwarzer, G., Schafer, K., Daschner, F. D., and Grundmann, H. (2000) Methicillin-resistant *Staphylococcus aureus* in a teaching hospital: investigation of a nosocomial transmission using a matched case-control study. *J. Hosp. Infect. 46*, 263–270.
(30) Welling, M. M., Lupetti, A., Balter, H. S., Lanzzeri, S., Souto, B., Rey, A. M., Savio, E. O., Paulusma-Annema, A., Pauwels, E. K. J., and Nivvering, P. H. (2001) ^{99m}Tc-labeled antimicrobial peptides for detection of bacterial and *Candida albicans* infections. *J. Nucl. Med. 42*, 788–794.

BC700376V